Cascading enables ultrafast gain recovery dynamics of quantum dot semiconductor optical amplifiers

Niels Majer, Kathy Lüdge, and Eckehard Schöll
Institut für Theoretische Physik, Technische Universität Berlin, D-10623 Berlin, Germany
(Received 27 August 2010; revised manuscript received 29 October 2010; published 1 December 2010)

In this work the ultrafast gain recovery dynamics of a quantum dot semiconductor optical amplifier is investigated on the basis of semiconductor Bloch equations including microscopically calculated carrier-carrier scattering rates between the two-dimensional carrier reservoir and the confined quantum dot ground and first excited state. By analyzing the different scattering contributions we show that the cascading process makes a major contribution to the ultrafast recovery dynamics.

DOI: 10.1103/PhysRevB.82.235301 PACS number(s): 78.67.Hc, 42.55.Px, 42.60.Rn

I. INTRODUCTION

Optoelectronic devices based on semiconductor quantum dots (QDs) are promising candidates for future high-speed telecom applications with low operation currents, high temperature stability, low chirp, and ultrafast gain recovery dynamics and hence pattern effect free amplification at high bit rates. Efficient carrier-carrier and carrier-phonon scattering processes into and between the discrete confined QD levels play a crucial role in the operation characteristics of QD-based devices and numerous experimental and theoretical investigations have addressed these topics. The simplest theoretical approach to carrier scattering is based on time-dependent perturbation theory containing energy conserving δ functions in terms of single-particle energies of the initial and final states.[1,2] In more elaborate quantum kinetic descriptions[3,4] the requirement of strict energy conservation is absent, which helps to resolve such issues as the phonon bottleneck[5,6] present in the simpler perturbative approaches.

In this paper we investigate the performance of QD semiconductor optical amplifiers (SOAs) by analyzing the gain recovery dynamics in response to ultrashort (150 fs) input pulses. Under high-injection currents the dominant contribution to carrier scattering into the QDs is given by carrier-carrier scattering (Auger) processes which we calculate using a time-dependent perturbative approach. Carrier-phonon scattering is implicitly included through the assumption of fast thermalization of carriers in the carrier reservoir. By including carrier-carrier scattering processes between the confined QD ground state (GS) and first excited state (ES) and the carrier reservoir, we extend our previous model which was restricted to the QD ground state.[7–10] The carrier reservoir is modeled by a two-dimensional (2D) quantum well (QW) into which carriers are injected and then scatter into the discrete QD levels. There is an ongoing discussion in the literature[11–14] whether direct capture or relaxation processes dominate the recovery dynamics of QD SOAs. In experiments[11,15,16] the gain recovery was found to be very fast (~ps). Including only the QD ground state in the carrier kinetics cannot account quantitatively for this behavior. Therefore in typical rate equation approaches a multitude of QD levels are considered[12] using numerical fits with constant transition rates between QW states and QD levels. In our approach we incorporate microscopically calculated Auger scattering contributions for transitions between GS, ES, and QW. This allows us to quantify the strength of the different scattering processes and we find that the cascading process via the excited state to the ground state of the quantum dot makes the major contribution to the ultrafast gain recovery dynamics observed in QD SOAs.

The paper is organized as follows. After introducing the theoretical model in Sec. II we present the microscopic approach to Auger scattering in Sec. III. In Sec. IV we discuss the impact of the various scattering channels to the gain recovery dynamics of the QD SOA and conclude in Sec. V.

II. MODEL

The theoretical model used to describe the QD SOA is based on a Bloch equation approach[17] for the coupled dynamics of the interband polarization and the electron (e) and hole (h) occupation probabilities of the QDs. We consider optical transitions between the electron and hole GS as well as the first ES of the QDs. Inhomogeneous broadening, which occurs in real devices due to fluctuations in QD size and material composition and directly affects the energy levels, is accounted for by assuming a Gaussian size distribution around a central ground-state transition frequency ω_0 with standard deviation δ_ω. The spectral QD density is then given by $N(\omega)=\frac{N^{\mathrm{QD}}}{\sqrt{2\pi}\delta_\omega}\exp[-\frac{(\omega-\omega_0)^2}{2\delta_\omega^2}]$ and the total QD density N^{QD} is approximated by a sum over a finite number of subensembles $N^{\mathrm{QD}}=\Sigma_j N^j=\Sigma_j N(\omega_j)\Delta\omega$, where $\Delta\omega$ denotes the spectral width of the QD subgroups. Furthermore, the separate dynamics of electrons and holes in the 2D carrier reservoir surrounding the QDs is taken into account in our modeling approach. Assuming an input light field of the form $E(t)=\frac{1}{2}E_0(t)[\exp(i\omega_L t)+\exp(-i\omega_L t)]$, where $E_0(t)$ is the slowly time varying envelope of the electric field and ω_L is the carrier-wave frequency, the set of equations in the usual slowly varying envelope and rotating wave approximation take the following form:

$$\frac{\partial p_m^j}{\partial t}=-i\delta\omega_m^j p_m^j-i\frac{\Omega}{2}(f_{e,m}^j+f_{h,m}^j-1)-\frac{1}{T_2}p_m^j, \qquad (1)$$

$$\frac{\partial f_{e,m}^j}{\partial t}=-\mathrm{Im}[\Omega p_m^{j*}]-R_{sp}+\left.\frac{\partial f_{e,m}^j}{\partial t}\right|_{col}, \qquad (2)$$

$$\frac{\partial f_{h,m}^{j}}{\partial t} = -\,\mathrm{Im}[\Omega p_m^{j*}] - R_{sp} + \left.\frac{\partial f_{h,m}^{j}}{\partial t}\right|_{col}, \tag{3}$$

$$\frac{\partial w_e}{\partial t} = \frac{j(t)}{e_0} - \tilde{R}_{sp} - 2\sum_{m,j} N^j \left.\frac{\partial f_{e,m}^{j}}{\partial t}\right|_{col}, \tag{4}$$

$$\frac{\partial w_h}{\partial t} = \frac{j(t)}{e_0} - \tilde{R}_{sp} - 2\sum_{m,j} N^j \left.\frac{\partial f_{h,m}^{j}}{\partial t}\right|_{col}. \tag{5}$$

Equations (1)–(3) constitute the semiconductor Bloch equations and Eqs. (4) and (5) are the dynamic equations for the QW carriers. The superscript j denotes the jth subgroup of QDs of the inhomogeneously broadened ensemble. The QD ground state and excited state are labeled by m. The microscopic polarization p_m^j is a dimensionless quantity describing the probability of an optical transition between the respective electron and hole levels. T_2 is the dephasing time of the optical polarization, which accounts for coherence loss through scattering processes. $f_{e,m}^j$ and $f_{h,m}^j$ are the electron and hole occupation probabilities of the jth subensemble of the mth QD level, and w_e and w_h are the electron and hole densities in the carrier reservoir, respectively. The total QD carrier density is obtained by summing over all subgroups, $n_{b,m}=2\Sigma_j f_{b,m}^j N^j$ for $b=e,h$. The factor of 2 arises due to spin degeneracy of the QD levels. The total macroscopic polarization density P is obtained by summing over all states and subensembles, $P=\Sigma_{j,m}\frac{N^j}{d}\mu p_m^j$, where d is the thickness of the active region. The detuning of the input light field frequency ω_L to the frequency ω_m^j of the optical transition of the respective QD level is given by $\delta\omega_m^j=(\omega_m^j-\omega_L)$. The Rabi frequency of the QD transitions with associated dipole moment μ (assumed to be equal for all QDs) is $\Omega(t)=\frac{\mu}{\hbar}E(t)$. $R_{sp}(f_{e,m}^j,f_{h,m}^j)=W_m f_{e,m}^j f_{h,m}^j$ is the spontaneous recombination rate with the Einstein coefficient $W_m=\frac{\mu^2\sqrt{\epsilon_{bg}}}{3\pi\epsilon_0\hbar}(\frac{\omega_m}{c})^3$ (background dielectric constant ϵ_{bg}, elementary charge e_0, and vacuum velocity of light c). An important contribution to the dynamics of QD SOAs is the nonradiative carrier-carrier scattering between confined QD states and continuous 2D QW states denoted by $(\partial/\partial t)f_{b,m}^j|_{col}$. The electric current density $j(t)$ is injected into the QW. The spontaneous QW band-band recombination rate is given by $\tilde{R}_{sp}=B^S w_e w_h$ with rate constant B^S. The InGaAs dot-in-a-well structure is modeled by a parabolic QW band structure with effective masses $m_e=0.043m_0$ and $m_h=0.45m_0$. The in-plane part of the QD wave functions is approximated by 2D harmonic-oscillator eigenfunctions, whereas the QW wave functions are approximated by orthogonalized plane waves. The confinement potential in z direction is treated in an effective-well-width approximation using an infinite potential barrier with width $L=8$ nm. A schematic energy diagram of the QD-QW system is shown in Fig. 1(a). The input pulse amplitude $E_0(t)$ is modeled as a Gaussian with a full width at half maximum (FWHM) of 150 fs. The parameters used in the simulation are listed in Table I.

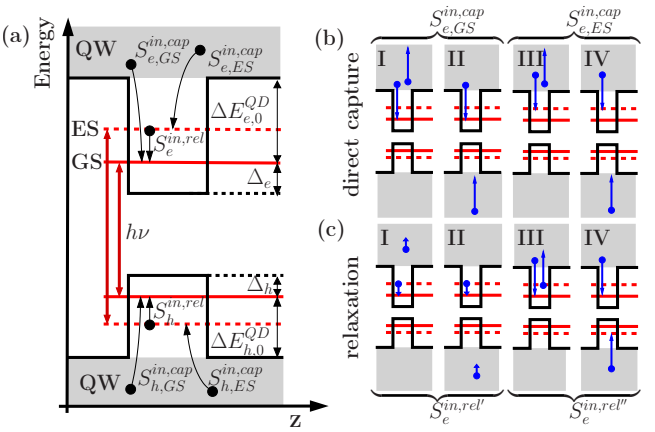

FIG. 1. (Color online) (a) Energy diagram of the QD-QW system. (b) Direct electron-capture processes from the QW to the QD ground state (I,II) and first-excited state (III,IV). Panels I, III and panels II, IV show pure e-e and mixed e-h scattering processes, respectively. (c) Electron relaxation processes to the QD ground state. (blue/dark gray arrows denote electron transitions also in the valence band).

III. AUGER SCATTERING PROCESSES

In a device operated under high-injection currents carrier-carrier scattering makes, next to carrier-phonon scattering, an important contribution to the interlevel carrier dynamics. In this paper we focus on an operating regime well above transparency, where we assume Coulomb scattering to make the dominant contribution to carrier scattering and therefore restrict the QD-QW scattering contributions to those resulting from carrier-carrier scattering. Carrier-phonon effects remain implicitly included in the fast thermalization of QW carriers. For the evaluation of the carrier-carrier scattering contributions we remain within the Markov limit since the total state space is in this case large enough to provide efficient scattering already with strict energy conservation (as opposed to carrier-phonon scattering, where a mismatch of the transition energy to the LO-phonon energy prohibits efficient scattering within the Markov limit and quantum kinetic theories predict

TABLE I. Numerical parameters used in the simulation unless stated otherwise.

Symbol	Value	Symbol	Value
$\Delta E_{e,m=0}^{\mathrm{QD}}$	210 meV	$\Delta E_{e,m=\pm1}^{\mathrm{QD}}$	146 meV
$\Delta E_{h,m=0}^{\mathrm{QD}}$	50 meV	$\Delta E_{h,m=\pm1}^{\mathrm{QD}}$	44 meV
Δ_e	64 meV	Δ_h	6 meV
d	4 nm	μ	$0.6e_0$ nm
$\hbar\delta_\omega$	4.25 meV	$\hbar\Delta\omega$	0.36 meV
$\hbar\omega_0=\hbar\omega_L$	0.96 eV	B^S	540 ns^{-1} nm^2
ϵ_{bg}	14.2	N^{QD}	10^{10} cm^{-2}
m_e	$0.043m_0$	m_h	$0.45m_0$
$W_{m=0}$, $W_{m=\pm1}$	0.7, 0.84 ns^{-1}	FWHM	150 fs
T_2	25 fs	Θ	π
j_0	1 A cm^{-2}	j	$1,\ldots,70$

larger scattering rates). The collision term in Eqs. (2)–(5) is given in the Markov limit up to second order in the screened Coulomb potential V by[2,18]

$$\left.\frac{\partial f^j_{b,m}}{\partial t}\right|_{col} = \frac{2\pi}{\hbar}\sum_{\nu_1\nu_2\nu_3} V_{\nu_1\nu_3\nu_2 m}[V^*_{\nu_1\nu_3\nu_2 m} - V^*_{\nu_3\nu_1\nu_2 m}] \times \delta(\epsilon_m - \epsilon_{\nu_1} + \epsilon_{\nu_2} - \epsilon_{\nu_3}) \times [f_{\nu_1}(1-f_{\nu_2})f_{\nu_3}(1-f^j_{b,m}) - (1-f_{\nu_1})f_{\nu_2}(1-f_{\nu_3})f^j_{b,m}] \quad (6)$$

with $b \in \{e,h\}$. In these Auger-type scattering events two carriers scatter from initial states ν_1 (with energy ϵ_{ν_1}) and ν_3 to final states m and ν_2, respectively, and vice versa. The calculation involves screened Coulomb matrix elements for the direct and exchange interaction $|V_{\nu_1\nu_3\nu_2 m}|^2$ and $V_{\nu_1\nu_3\nu_2 m}V^*_{\nu_3\nu_1\nu_2 m}$, respectively. Details of the explicit form of the Coulomb matrix elements and the involved wave functions can be found in the Appendix. The index m represents the quantum number of the 2D angular momentum of the confined QD states, $m=0$ and $m \in \{1,-1\}$ for the GS and ES, respectively. The δ function in Eq. (6) ensures energy conservation. The occupation probability of state ν_i is denoted by f_{ν_i}. Figures 1(b) and 1(c) give a systematic overview of all processes leading to in-scattering into the QD electron levels. The blue (dark gray) arrows denote electron transitions of the scattering partners. Panels I and III show pure e-e processes while panels II and IV display mixed e-h processes. The corresponding processes for in-scattering into the QD hole levels are obtained by exchanging all electron and hole states. The out-scattering processes are obtained by inverting all arrows of the electron transitions. The exchange processes of pure e-e capture processes contributing to the scattering rates are not shown since there is no qualitative difference to the direct processes. In case of mixed e-h processes (II, IV) the exchange processes lead to transitions across the band gap that are neglected since they are unlikely to occur. Note that the process shown in panel III of Fig. 1(c) is the exchange process of the one in panel I. In the following we decompose the scattering rate into contributions originating from direct carrier capture from the QW into the GS and ES (R^{cap}) and relaxation processes from ES to GS ($R^{rel'}$,$R^{rel''}$) as shown in Figs. 1(b) and 1(c), respectively. The relaxation processes are split into scattering events with one intra-QD transition and a QW transition ($R^{rel'}$) and processes where both involved carriers perform transitions from QW states to QD states ($R^{rel''}$), i.e., $(\partial/\partial t)f^j_{b,m}|_{col} = R^{cap} + R^{rel'} + R^{rel''}$. Processes involving three QD states are neglected since energy conservation allows at most one k state in the QW to be involved thus inhibiting efficient scattering.

A. Direct capture

The contribution to Eq. (6) from direct capture processes [Fig. 1(b)] can be expressed as

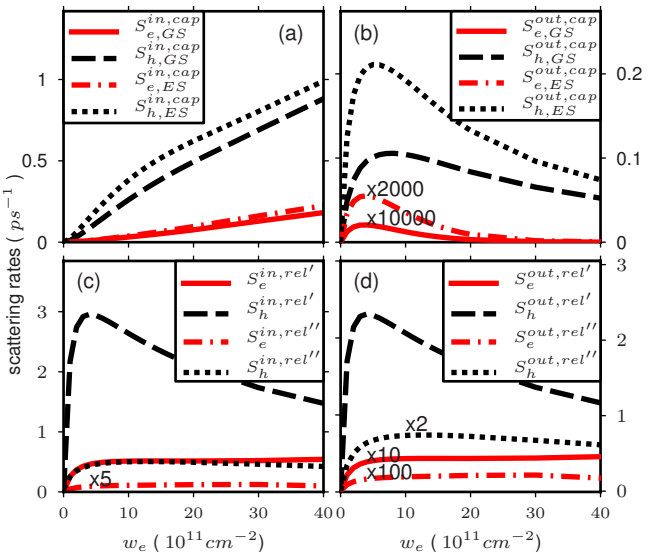

FIG. 2. (Color online) Auger scattering rates of the QD-QW system vs QW electron density $w_e(w_h/w_e=1.5)$. [(a) and (b)] Direct capture rates. [(c) and (d)] Intra-QD relaxation rates. Parameters see Table I.

$$R^{cap} = S^{in,cap}_{b,m}(1-f^j_{b,m}) - S^{out,cap}_{b,m}f^j_{b,m} \quad (7)$$

with the in-scattering rate $(k_1 \to m, k_3 \to k_2)$, where states in the QW are labeled by the in-plane carrier momentum k_i,

$$S^{in,cap}_{b,m} = \frac{2\pi}{\hbar}\sum_{k_1k_2k_3b'} V_{k_1k_3k_2m}[2V^*_{k_1k_3k_2m} - \delta_{b,b'}V^*_{k_3k_1k_2m}] \times \delta(\epsilon^b_m - \epsilon^b_{k_1} + \epsilon^{b'}_{k_2} - \epsilon^{b'}_{k_3})f_{k_1}(1-f_{k_2})f_{k_3}. \quad (8)$$

The respective out-scattering rate is obtained by the substitution $f_{k_i} \to (1-f_{k_i})$ in Eq. (8). Assuming quasi-equilibrium within the QW system, the in- and out-scattering rates are related to each other via detailed balance,[7]

$$S^{in,cap}_{b,m} = S^{out,cap}_{b,m}\exp\left(\frac{\mp\Delta E^{QD}_{b,m} \pm F^{QW}_b}{kT}\right), \quad (9)$$

where F^{QW}_b are the quasi-Fermi levels in the QW and the upper and lower signs refer to $b=e$ and $b=h$, respectively. The calculated direct capture rates as a function of the QW carrier densities are shown in Figs. 2(a) and 2(b). For low densities the in-scattering rates show a quadratic increase with growing QW carrier densities as expected from mass action kinetics. With increasing w_b deviations from this behavior become apparent eventually leading to a decrease in the scattering rates due to Pauli blocking [see red dashed-dotted line in Fig. 2(a)]. The out-scattering rates are characterized by a sharp increase followed by a decrease due to Pauli blocking at higher densities.

B. Relaxation processes

The relaxation processes shown in Fig. 1(c) describe a redistribution of carriers within the intra-QD levels. The in-scattering rate $(m_1 \to m, k_3 \to k_2)$ for processes I and II with

$m_1 \in \{-1,1\}$, $m=0$, contributing to Eq. (6), is given by

$$S^{in,rel'}_{b,m} = \frac{2\pi}{\hbar} \sum_{k_2 k_3 b'} V_{m_1 k_3 k_2 m}[2V^*_{m_1 k_3 k_2 m} - \delta_{b,b'} V^*_{k_3 m_1 k_2 m}] \times \delta(\epsilon^b_m - \epsilon^b_{m_1} + \epsilon^{b'}_{k_2} - \epsilon^{b'}_{k_3})(1-f_{k_2})f_{k_3},$$

$$R^{rel'} = S^{in,rel'}_{b,m} f^j_{b,m_1}(1-f^j_{b,m}) - S^{out,rel'}_{b,m}(1-f^j_{b,m_1})f^j_{b,m}. \quad (10)$$

The dynamical equations for the processes III and IV ($R^{rel''}$) in Fig. 1(c) can be obtained in a similar fashion as Eq. (10) with the difference that pure (e-e, h-h) and mixed (e-h) processes have to be separated, as the QD occupation factors involve the carrier types of both involved scattering partners. The rate for the mixed case is vanishingly small and the shown rate is the one for the pure case. For electrons it reads:

$$S^{in,rel''}_{e,m} = \frac{2\pi}{\hbar} \sum_{k_1 k_2} V_{k_1 m_1 k_2 m}[2V^*_{k_1 m_1 k_2 m} - V^*_{m_1 k_1 k_2 m}] \times \delta(\epsilon^e_m - \epsilon^e_{m_1} + \epsilon^e_{k_2} - \epsilon^e_{k_1})(1-f_{k_2})f_{k_1},$$

$$R^{rel''} = S^{in,rel''}_{e,m} f^j_{e,m_1}(1-f^j_{e,m}) - S^{out,rel''}_{e,m}(1-f^j_{e,m_1})f^j_{e,m}. \quad (11)$$

The calculated rates are shown in Figs. 2(c) and 2(d). The relaxation rates of type $S^{rel'}$ are characterized by a sharp increase and a decrease at higher densities due to the effect of Pauli blocking. Note that in- and out-scattering rates only differ by a constant factor $S^{out,rel}_{e/h} = S^{in,rel}_{e/h} \exp[-\Delta_{e/h}/(k_B T)]$ resulting from detailed balance.

IV. GAIN RECOVERY DYNAMICS

A key parameter determining the performance of an SOA is the gain recovery time after an input light pulse with pulse area $\theta = \int \Omega dt$ has depleted the carriers. This can be determined by a pump-probe experiment, where a probe pulse measures the gain after a delay time τ with respect to the pump pulse. The gain of the probe pulse can be approximated by $g(\omega,\tau) = -\omega\, \mathrm{Im}[\frac{P_{probe}(\omega,\tau)}{E_{probe}(\omega)}]$. Here, P_{probe} and E_{probe} are the Fourier amplitudes of the macroscopic polarization and the probe pulse electric field, respectively. The input light field is chosen as resonant to the central ground-state transition of the QDs. Our microscopic approach now allows for an analysis of the influence of different scattering channels on the gain recovery dynamics of a QD SOA. In Figs. 3 and 4 we show the calculated gain recovery and the associated carrier dynamics for three different scenarios sketched in Fig. 3(b). Scenario 1 allows only direct capture to the QD ground and excited state while scenario 2 allows the carriers to relax to the QD ground state via a cascading process. Scenario 3 includes both cascading and direct capture. Figure 3(a) shows the normalized gain in dependence of the pump-probe delay time τ for the three scenarios depicted in Fig. 3(b). All curves show maximum gain depletion for a pump-probe delay time $\tau=0$. Scenario 2 deviates only slightly from scenario 3 in the intermediate recovery stage, whereas the coherent recovery phase ($\tau \leq 100$ fs) perfectly coincides. If the relaxation path from the excited state to the ground state is blocked (scenario 1) the recovery dynamics drastically deteriorates compared to the two other scenarios. The initial gain depletion around $\tau=0$ is stronger and the normalized gain recovers much more slowly than in the other scenarios for $\tau>0$. The population dynamics of the QD electrons and holes for scenario 1 with pump-probe delay $\tau=0$ is shown in Figs. 4(a) and 4(b), respectively, while Figs. 4(c) and 4(d) depict the electron and hole dynamics for scenario 3. In Figs. 4(a) and 4(b), the resonant interaction of the QD ground state with the incoming light field causes a strong carrier depletion both of electrons and holes, whereas the off-resonant ES experiences only little light-matter interaction and the relaxation path to the GS is blocked. In Figs. 4(c) and 4(d) relaxation processes between the ES and GS are allowed resulting in a strong decrease in the ES carrier populations and a faster refilling of the GS compared to scenario 1. The corresponding time evolution of the QW carrier densities for scenarios 1 and 3 is plotted in Fig. 5. The recovery dynamics of the carrier reservoir is on a nanosecond rather than a picosecond

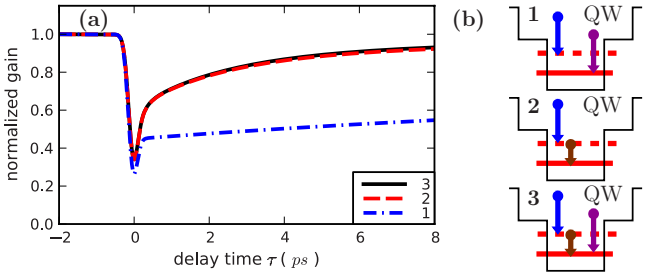

FIG. 3. (Color online) Gain recovery dynamics for scattering scenarios 1 (direct capture), 2 (cascading), and 3 (all) as sketched in panel (b) (Auger electrons omitted). Parameters: $j \approx 10 j_0$, see also Table I.

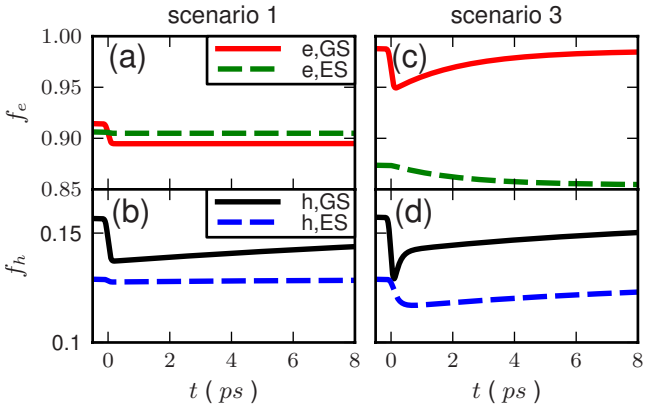

FIG. 4. (Color online) Average [(a) and (b)] electron and [(b) and (d)] hole population vs time for pump-probe delay $\tau=0$ for direct capture processes only [scenario 1 in Fig. 3(b)] and with all Auger processes [scenario 3 in Fig. 3(b)], respectively. Red/gray (black) solid curves are ground-state electron (hole) populations, and green/light gray (blue/dark gray) dashed curves are excited-state populations. Parameters as in Fig. 3.

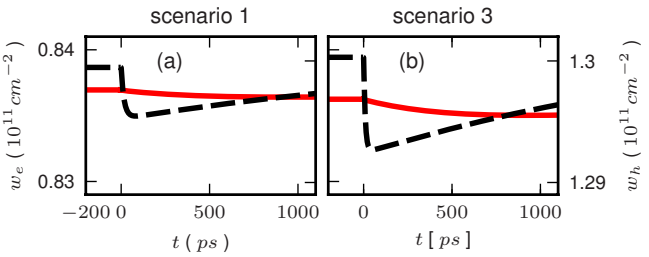

FIG. 5. (Color online) (a) Time traces of w_e (red solid, left axis) and w_h (black dashed, right axis) for scenario 1 of Fig. 3(b). (b) Same for scenario 3. Parameters as in Fig. 3.

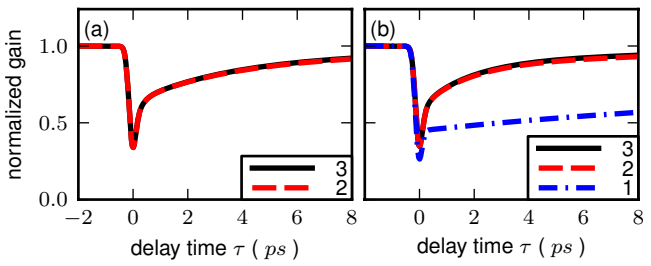

FIG. 6. (Color online) Gain recovery dynamics for scattering scenarios 1 (direct capture), 2 (cascading), and 3 (all) as sketched in panel (b) of Fig. 3 for (a): injection current density $j=5j_0$ and (b): injection current density $j=20j_0$. Parameters: see Table I.

time scale (as for the QD carriers). Again, comparing scenarios 1 and 3 the carrier dynamics differs qualitatively. With the additional relaxation channel (scenario 3), the carrier drain from the QW is stronger, the maximum depletion is higher, and it occurs earlier. This is due to stronger accumulated scattering into the QDs. The nonlinearity of carrier-carrier scattering, especially due to Pauli blocking effects, could potentially shift the relative importance of different scattering channels for changing QW carrier densities. In Fig. 6 the gain recovery dynamics is plotted for different injection current densities of $j=5j_0$ and $j=20j_0$. While the gain recovers faster in the case of higher injection current [panel (b)], the cascading process remains the key channel in the gain recovery. The direct capture process in panel (a) is omitted because for the given injection current density the QD ground state is not in an inverted state.

V. CONCLUSION

In conclusion, our systematic microscopic analysis of different Auger scattering channels, including confined QD ground and excited states and extended QW states, combined with a full nonlinear simulation of the coupled polarization and population dynamics of carriers has established that cascading Coulomb scattering processes from the carrier reservoir via the QD excited state into the QD ground state constitute the major contribution to the ultrafast recovery dynamics of QD SOAs.

ACKNOWLEDGMENTS

This work was supported by DFG in the framework of Sfb 787. We thank A. Knorr and U. Woggon for useful discussions. In addition we thank A. Wilms for helpful comments regarding the calculation of the Coulomb scattering rates.

APPENDIX: MATRIX ELEMENTS AND ORTHOGONALIZATION PROCEDURE

The matrix elements of the Coulomb potential from Eq. (6),

$$V_{\nu_1\nu_3\nu_2\nu} = \int d^3r d^3r' \Psi^*_{\nu}(\mathbf{r}) \Psi^*_{\nu_2}(\mathbf{r}') \frac{e_0^2}{4\pi\epsilon_0 r} \Psi_{\nu_1}(\mathbf{r}) \Psi_{\nu_3}(\mathbf{r}') \tag{A1}$$

involve the single-particle wave functions $\Psi_{\nu}(\mathbf{r})$ of electrons and holes in the confinement potential of the QD-QW system. Under the assumption that the wave functions can be separated into an in-plane component and a perpendicular (z) component $\Psi_{\nu}(\mathbf{r}) = \phi^b_l(\rho)\xi^b_\sigma(z)u_b(\mathbf{r})$, where $u_b(\mathbf{r})$ are the lattice Bloch functions and l and σ the quantum numbers of the in-plane and z-component wave functions, respectively, Eq. (A1) can be expressed as[2]

$$V_{\nu_1\nu_3\nu_2\nu} = \frac{1}{A}\sum_q V^{b,b_2}_{\sigma_1\sigma_3\sigma_2\sigma} \delta_{b,b_1}\delta_{b_2,b_3} \times \langle \phi^b_l | e^{-i\mathbf{q}\cdot\rho} | \phi^{b_1}_{l_1} \rangle \langle \phi^{b_2}_{l_2} | e^{i\mathbf{q}\cdot\rho} | \phi^{b_3}_{l_3} \rangle, \tag{A2}$$

where $\mathbf{q}$ is the two-dimensional in-plane carrier momentum and

$$V^{b,b_2}_{\sigma_1\sigma_3\sigma_2\sigma} = \frac{e_0^2}{2\epsilon_0 q} \int dz dz' \times \xi^b_\sigma(z)^* \xi^{b'}_{\sigma_2}(z')^* e^{-q|z-z'|} \xi^{b'}_{\sigma_3}(z) \xi^b_{\sigma_1}(z'). \tag{A3}$$

In a simple approach to the QD confinement we approximate the z-confinement potential by an infinite-height potential barrier of width $L=2d$, where d is the thickness of the QW layer. For the in-plane confinement potential of the QDs we adopt the model of a two-dimensional harmonic oscillator allowing for an analytic solution of the wave function overlap integrals in Eq. (A2). The calculation of realistic single-particle wave functions is a task of its own and requires detailed knowledge of the QD geometry and the material composition and is beyond the scope of this paper. In a quantum well containing no QDs the in-plane component of the wave functions would be plane waves $\phi^0_{\mathbf{k}}(\sigma) = (1/\sqrt{A})e^{i\mathbf{k}\cdot\sigma}$. In the presence of QDs the QW wave functions are altered in the vicinity of the QDs due to local changes in the QD-QW potential. To describe the combined system we therefore use plane waves orthogonalized with respect to the QD states (OPW)

$$|\phi_{\mathbf{k}}\rangle = \frac{1}{N_{\mathbf{k}}}\left(|\phi^0_{\mathbf{k}}\rangle - \sum_\alpha |\phi_\alpha\rangle\langle\phi_\alpha|\phi^0_{\mathbf{k}}\rangle \right), \tag{A4}$$

where $N_{\mathbf{k}}$ is the normalization constant. The summation runs over all localized QD states. Assuming an ensemble of identical QDs located at positions $\{\sigma_i\}$ with nonoverlapping

wave functions $\phi_m^i(\sigma)$ the summation runs over $\alpha=(m,i)$. By construction, the OPW states are orthogonal to all QD states. The orthogonality of different OPW states can be obtained for an ensemble of randomly distributed QDs in the large area limit, meaning that both the in-plane area $A\to\infty$ and the number of QDs $N\to\infty$ such that the QD density remains constant ($N/A=$const). In that case only the QW densities appear in the evaluation of Eq. (A2).

[1] H. C. Schneider, W. W. Chow, and S. W. Koch, Phys. Rev. B **64**, 115315 (2001).

[2] T. R. Nielsen, P. Gartner, and F. Jahnke, Phys. Rev. B **69**, 235314 (2004).

[3] M. Lorke, T. R. Nielsen, J. Seebeck, P. Gartner, and F. Jahnke, Phys. Rev. B **73**, 085324 (2006).

[4] M. Lorke, F. Jahnke, and W. W. Chow, Appl. Phys. Lett. **90**, 051112 (2007).

[5] J. Seebeck, T. R. Nielsen, P. Gartner, and F. Jahnke, Phys. Rev. B **71**, 125327 (2005).

[6] H. Kurtze, J. Seebeck, P. Gartner, D. R. Yakovlev, D. Reuter, A. D. Wieck, M. Bayer, and F. Jahnke, Phys. Rev. B **80**, 235319 (2009).

[7] K. Lüdge and E. Schöll, IEEE J. Quantum Electron. **45**, 1396 (2009).

[8] K. Lüdge and E. Schöll, Eur. Phys. J. D **58**, 167 (2010).

[9] C. Otto, K. Lüdge, and E. Schöll, Phys. Status Solidi B **247**, 829 (2010).

[10] M. Wegert, N. Majer, K. Lüdge, S. Dommers-Völkel, J. Gomis-Bresco, A. Knorr, U. Woggon, and E. Schöll, Semicond. Sci. Technol. **26**, 014008 (2011).

[11] J. Gomis-Bresco, S. Dommers, V. V. Temnov, U. Woggon, J. Martinez-Pastor, M. Laemmlin, and D. Bimberg, IEEE J. Quantum Electron. **45**, 1121 (2009).

[12] J. Kim, C. Meuer, D. Bimberg, and G. Eisenstein, Appl. Phys. Lett. **94**, 041112 (2009).

[13] A. V. Uskov, T. W. Berg, and J. Mørk, IEEE J. Quantum Electron. **40**, 306 (2004).

[14] G. Bertrand, C. Delage, M. Bafleur, N. Nolhier, J.-M. Dorkel, Q. Nguyen, N. Mauran, D. Trémouilles, and P. Perdu, IEEE J. Solid-State Circuits **36**, 1373 (2001).

[15] J. Gomis-Bresco, S. Dommers, V. V. Temnov, U. Woggon, M. Laemmlin, D. Bimberg, E. Malic, M. Richter, E. Schöll, and A. Knorr, Phys. Rev. Lett. **101**, 256803 (2008).

[16] P. Borri, W. Langbein, J. M. Hvam, F. Heinrichsdorff, M.-H. Mao, and D. Bimberg, IEEE Photon. Technol. Lett. **12**, 594 (2000).

[17] W. W. Chow and S. W. Koch, *Semiconductor-Laser Fundamentals* (Springer, New York, 1999).

[18] H. H. Nilsson, J. Z. Zhang, and I. Galbraith, Phys. Rev. B **72**, 205331 (2005).